JACC: CARDIOVASCULAR IMAGING VOL. 14, NO. 9, 2021

ORIGINAL RESEARCH

Clinical Validation of a 3-Dimensional Ultrafast Cardiac Magnetic Resonance Protocol Including Single Breath-Hold 3-Dimensional Sequences

Sandra Gómez-Talavera, MD,[a,b,c,*] Rodrigo Fernandez-Jimenez, MD, PhD,[a,c,d,*] Valentín Fuster, MD, PhD,[a,e] Nils D. Nothnagel, PhD,[f] Marc Kouwenhoven, PhD,[g] Matthew Clemence, PhD,[h] Inés García-Lunar, MD,[a,c,i] María C. Gómez-Rubín, MD,[j] Felipe Navarro, MD, PhD,[b,c] Braulio Pérez-Asenjo, BPT, RT,[a] Leticia Fernández-Friera, MD, PhD,[a,c,k] María J. Calero, MD,[l] Miguel Orejas, MD, PhD,[b] José A. Cabrera, MD, PhD,[i] Manuel Desco, MD, PhD,[a,m] Gonzalo Pizarro, MD, PhD,[a,c,i] Borja Ibáñez, MD, PhD,[a,b,c] Javier Sánchez-González, PhD[f]

ABSTRACT

OBJECTIVES This study sought to clinically validate a novel 3-dimensional (3D) ultrafast cardiac magnetic resonance (CMR) protocol including cine (anatomy and function) and late gadolinium enhancement (LGE), each in a single breath-hold.

BACKGROUND CMR is the reference tool for cardiac imaging but is time-consuming.

METHODS A protocol comprising isotropic 3D cine (Enhanced sensitivity encoding [SENSE] by Static Outer volume Subtraction [ESSOS]) and isotropic 3D LGE sequences was compared with a standard cine+LGE protocol in a prospective study of 107 patients (age 58 ± 11 years; 24% female). Left ventricular (LV) mass, volumes, and LV and right ventricular (RV) ejection fraction (LVEF, RVEF) were assessed by 3D ESSOS and 2D cine CMR. LGE (% LV) was assessed using 3D and 2D sequences.

RESULTS Three-dimensional and LGE acquisitions lasted 24 and 22 s, respectively. Three-dimensional and LGE images were of good quality and allowed quantification in all cases. Mean LVEF by 3D and 2D CMR were 51 ± 12% and 52 ± 12%, respectively, with excellent intermethod agreement (intraclass correlation coefficient [ICC]: 0.96; 95% confidence interval [CI]: 0.94 to 0.97) and insignificant bias. Mean RVEF 3D and 2D CMR were 60.4 ± 5.4% and 59.7 ± 5.2%, respectively, with acceptable intermethod agreement (ICC: 0.73; 95% CI: 0.63 to 0.81) and insignificant bias. Both 2D and 3D LGE showed excellent agreement, and intraobserver and interobserver agreement were excellent for 3D LGE.

CONCLUSIONS ESSOS single breath-hold 3D CMR allows accurate assessment of heart anatomy and function. Combining ESSOS with 3D LGE allows complete cardiac examination in <1 min of acquisition time. This protocol expands the indication for CMR, reduces costs, and increases patient comfort. (J Am Coll Cardiol Img 2021;14:1742–1754) © 2021 The Authors. Published by Elsevier on behalf of the American College of Cardiology Foundation. This is an open access article under the CC BY-NC-ND license (http://creativecommons.org/licenses/by-nc-nd/4.0/).

From [a]Clinical Research Department, Centro Nacional de Investigaciones Cardiovasculares (CNIC), Madrid, Spain; [b]Department of Cardiology, IIS-Hospital Fundacion Jiménez Díaz, Madrid, Spain; [c]CIBER de Enfermedades Cardiovasculares (CIBERCV), Madrid, Spain; [d]Department of Cardiology, Hospital Universitario Clinico San Carlos, Madrid, Spain; [e]Department of Cardiology, Icahn School of Medicine at Mount Sinai, New York, New York, USA; [f]Clinical Science, Philips Healthcare Iberia, Madrid, Spain; [g]Clinical Science, Philips Healthcare, Best, the Netherlands; [h]Clinical Science, Philips Healthcare, Guildford, United Kingdom; [i]Department of Cardiology, Hospital Universitario Quiron UEM, Madrid, Spain; [j]Department of Cardiology, Hospital Ruber Juan Bravo UEM, Madrid, Spain; [k]Department of Cardiology, Hospital Montepríncipe-CEU, Madrid, Spain; [l]Department of Cardiology, Hospital Universtario Rey Juan Carlos-Móstoles, Madrid, Spain; and [m]Departamento de Bioingeniería e Ingeniería Aerospacial, Universidad Carlos III, Madrid, Spain. *Drs. Gómez-Talavera and Fernandez-Jimenez contributed equally to this work.

ISSN 1936-878X https://doi.org/10.1016/j.jcmg.2021.02.031

Cardiac magnetic resonance (CMR) is the reference method for noninvasive evaluation of the anatomy and function of the heart (1). Two of the key variables measured by CMR are left ventricular ejection fraction (LVEF) and the extent of injured myocardium (infarct size), both of which have important diagnostic and prognostic implications (1,2). Standard clinical CMR protocols include the acquisition of a first set of localization/scout images followed by the assessment of ventricular mass, volumes, and ejection fraction using 2-dimensional (2D) cine imaging. The presence and extent of injured myocardium are normally assessed by 2D late gadolinium enhancement (LGE) sequences approximately 10 min after administration of intravenous contrast agent (3). The practical application of clinical CMR protocols is associated with a number of difficulties. One such difficulty is correct adjustment of plane orientations for cardiac slice angulation, a highly specialized skill that requires extensive training. Another challenge is the long scan time. "Complete" left ventricular (LV) coverage requires the acquisition of 8 to 15 short-axis images, with each acquisition requiring a breath-hold of ~8 s (4). The long scan time is frequently associated with patient discomfort and claustrophobia, in some instances precluding a complete study. Moreover, the long time required for a complete basic cine and gadolinium-enhanced study is associated with high costs. Overall, these limitations result in CMR underuse in daily practice.

Recent technical developments have attempted to overcome these barriers and accelerate image acquisition (5,6). However, these innovations come at the cost of reducing image resolution or involve complex localization/scout imaging and time-consuming image reconstruction processes. Novel CMR approaches are needed to establish CMR as a convenient tool in standard clinical practice. The goal of this study was to validate a novel 3D ultrafast CMR protocol for assessing important cardiac variables (anatomy, function, and LGE). We prospectively enrolled 107 patients with a clinical indication for contrast-enhanced CMR imaging. The patients were analyzed by standard 2D CMR and with a new ultrafast 3-dimensional (3D) cine sequence (Enhanced sensitivity encoding [SENSE] by Static Outer volume Subtraction [ESSOS]).

METHODS

STUDY DESIGN, SETTING, AND PARTICIPANTS. Patients with a clinical indication for gadolinium-contrast enhanced CMR were prospectively recruited from 4 hospitals in Madrid, Spain. Patients eligible for enrollment were age ≥18 years with any of the following diagnoses: ST-segment elevation acute myocardial infarction successfully treated in the preceding 8 weeks; LV systolic dysfunction defined by LVEF <50% in a recent echocardiogram (in the preceding 4 weeks); right ventricular (RV) systolic dysfunction defined by tricuspid annular plane systolic excursion <15 mm in a recent echocardiogram (in the preceding 4 weeks); a previous diagnosis of hypertrophic cardiomyopathy, arrhythmogenic RV cardiomyopathy, or cardiac amyloidosis, regardless of systolic function; ascending aorta dilation >40 mm detected by echocardiography or computed tomography angiography. Exclusion criteria were pregnancy, presence of metallic objects or devices incompatible with CMR imaging, known allergy to gadolinium-based contrast agents, creatinine clearance ≤30 ml/min, permanent atrial fibrillation, severe chronic obstructive pulmonary disease, or known severe claustrophobia.

Ten additional patients underwent only the 3D ultrafast CMR protocol for its real-life testing and to estimate the door-to-door time. In the 10-patient, 3D ultrafast CMR protocol only, the contrast agent was administered just before the patient entered the magnet suite.

CMR examinations were conducted at the Centro Nacional de Investigaciones Cardiovasculares. In all patients, standard 2D cine imaging was followed by intravenous administration of weight-adjusted gadolinium-based contrast agent and the acquisition of 3D cine (ESSOS) and 3D LGE images and 2D LGE images (**Figure 1**). The study was approved by the Ethics Committee of the Hospital Universitario Fundación Jimenez Diaz and was conducted in accordance with guidelines on research involving human participants. All patients gave written informed consent to participate in the study.

ABBREVIATIONS AND ACRONYMS

2D = 2-dimensional
3D = 3-dimensional
CI = confidence interval
CMR = cardiac magnetic resonance
ESSOS = Enhanced sensitivity encoding (SENSE) by Static Outer volume Subtraction
FOV = field of view
ICC = intraclass correlation coefficient
LGE = late gadolinium enhancement
LV = left ventricle
LVEDV = left ventricular end-diastolic volume
LVEF = left ventricular ejection fraction
LVESV = left ventricular end-systolic volume
RV = right ventricle
RVEDV = right ventricular end-diastolic volume
RVEF = right ventricular ejection fraction
RVESV = right ventricular end-systolic volume
TFE = turbo field echo

The authors attest they are in compliance with human studies committees and animal welfare regulations of the authors' institutions and Food and Drug Administration guidelines, including patient consent where appropriate. For more information, visit the Author Center.

Manuscript received May 5, 2020; revised manuscript received January 5, 2021, accepted February 5, 2021.

FIGURE 1 Study Design

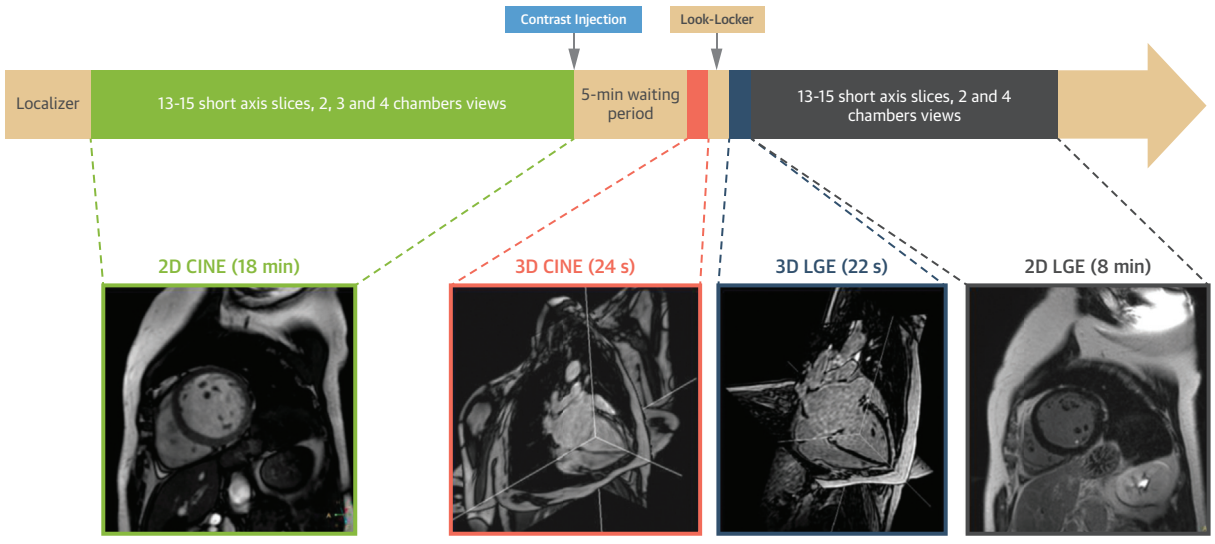

2D = 2-dimensional; 3D = 3-dimensional; LGE = late gadolinium enhancement.

IMAGING PROTOCOL. CMR examinations were conducted using a Philips 3-T Achieva Tx whole-body scanner (Philips Healthcare, Best, the Netherlands) equipped with a 16-element phased-array torso-cardiac coil. Standard multislice 2D cine CMR images were acquired before gadolinium-based contrast administration using a balanced turbo field echo (TFE), steady-state, free-precession sequence with the following parameters: field of view (FOV), 380 × 330 mm; voxel size, 1.7 × 2.0 mm; TR, 2.7 ms; TE, 1.35 ms; flip angle, 40°; and number of cardiac phases, 30. To reduce scan time, a parallel acquisition factor of 2 was applied in the phase-encoding direction. Initially, several scans were acquired to determine the correct short-axis orientation of the 2D short-axis dataset. The entire LV was covered by 13 to 15 slices, with slice thickness of 8 mm and no gap between slices.

The new 3D cine imaging sequence (ESSOS) was acquired after intravenous administration of 0.10 mmol/kg gadoteric acid contrast agent using a nonangulated 3D coronal volume with FOV of 300 × 520 × 310 mm (FH-LR-AP) and a readout direction in FH (bandwidth = 2,160 Hz/pixel). The 3D k-space was acquired using centric spiral ky-kz profile order with a voxel size of 2.6 × 2.6 × 2.6 mm (reconstructed to 2.0 × 2.0 × 2.0 mm) and 16 cardiac phases (triggered retrospectively). A detailed video of k-space filling from a real case can be found in Video 1. Nonselective radiofrequency excitation pulses were used to obtain a short TR (2.36 ms) with a relatively high flip angle (42°) while using full echo acquisition (TE = 1.18 ms). Net scan acceleration factor was 34 resulting from an ESSOS acceleration of 19.2 (6.0 × 3.2 in LR and AP direction) and halfscan factor of 0.56 (0.75 × 0.75 in LR and AP direction). The theory and technical aspects of the ESSOS approach are described in detail in the Supplemental Appendix and Supplemental Figures 1 to 4. In brief, ESSOS reconstruction is based on the acquisition of 2 interleaved datasets, one static and the other dynamic. The static dataset is acquired with a relatively low SENSE factor and is acquired only once in the cardiac cycle because it requires no temporal information. The dynamic (cine) dataset is acquired with a higher SENSE factor, for each cardiac phase. ESSOS automatically selects static region in the image domain and subtracts those regions from the dynamic dataset. After subtraction, the dynamic dataset is reconstructed and added to the static region in the image domain. After static region subtraction, dynamic regions covered a smaller volume in the FOV, resulting in a reduced effective SENSE factor.

Immediately after 3D cine ESSOS, look-locker scan was performed to determine the adequate inversion time to acquire 3D and 2D LGE images. Three-dimensional LGE imaging was conducted in the sagittal orientation using inversion recovery spoiled TFE acquisition (TR = 2.3 ms; TE = 1.1 ms; flip angle = 7°). A 3D volume of 300 × 150 × 320 mm

FIGURE 2 **Participant Flow Diagram**

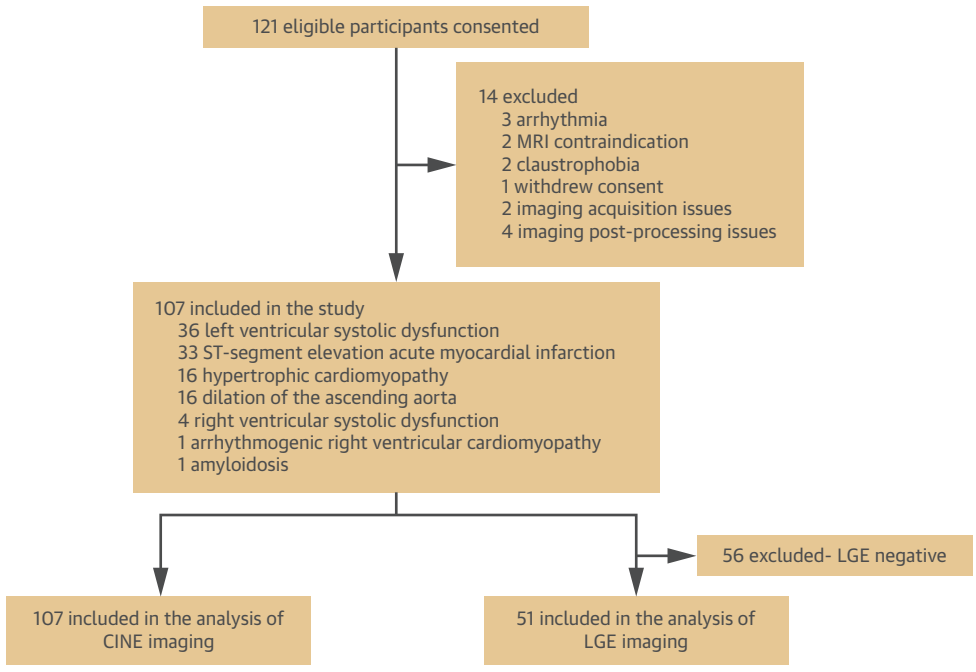

LGE= late gadolinium enhancement; MRI = magnetic resonance imaging.

(FH-LR-AP) was acquired with spatial resolution of $2.22 \times 2.22 \times 2.22$ mm^3. The acquisition was triggered at end-diastole with a mean shot interval of 185 ms, and the whole acquisition was accelerated using a parallel acquisition factor of 4 (2×2 in AP and LR), resulting in a breath-hold time of 22 s. For comparison, multiple 2D slices were acquired with equivalent acquisition technique. The in-plane resolution of 2D images was 1.55×0.55 mm, slice thickness was 8 mm, and images were acquired with FOV of 380×380 mm and parallel acquisition factor of 2, resulting in a 15-s breath-hold per slice.

IMAGE ANALYSIS. In all cardiac phases, 3D cine images were reformatted by an expert technician in the short-axis view using slice thickness of 8 mm with no gap, mimicking the coverage of 2D cine images. CMR images were analyzed with cardiac analysis software (IntelliSpace Portal 10, Philips Haifa, Haifa, Israel) by 2 independent experienced observers from the Centro Nacional de Investigaciones Cardiovasculares core imaging laboratory. LV mass, LV and RV volumes, and LVEF and right ventricular ejection fraction (RVEF) were obtained from 2D cine and 3D cine images, whereas the extent of LGE myocardium was obtained from 2D and 3D LGE images. Image quality was ranked in 4 different categories: 1) poor (not useful for clinical diagnosis); 2) regular (images valuable for clinical diagnosis but contain some artifacts); 3) good (valuable for clinical diagnosis without artifacts but have moderate spatial resolution or signal to noise); and 4) very good (optimal image quality).

In each cine image, LV endocardial borders were automatically traced with manual adjustment to obtain left ventricular end-diastolic volume (LVEDV), left ventricular end-systolic volume (LVESV), and LVEF. In the tracing convention used, the papillary muscles were included as part of the LV cavity volume. LV epicardial borders were traced on end-diastolic images, to measure LV volume, and on end-systolic images, to measure wall thickening. LV mass was obtained by multiplying LV volume by myocardial density (1.05 g/ml). Wall thickening was computed as the difference between the wall thickness at systolic and diastolic cardiac phases. To assess regional contractibility mean wall thickening, values were reported following the 16-segment American Heart Association model (7). Wall thickening analysis was performed in those participants with confirmed enhanced regions in the LGE. RV endocardial borders

TABLE 1 Absolute-Agreement and Consistency-of-Agreement ICC and 95% CI for Comparisons Between 2D and 3D Cine and LGE Measurements

Measured Variable	n	ICC	
		Absolute Agreement (95% CI)	Consistency of Agreement (95% CI)
LVEF, %	107	0.96 (0.94-0.97)	0.96 (0.94-0.97)
LVEDV, ml	107	0.93 (0.84-0.97)	0.95 (0.93-0.97)
LVESV, ml	107	0.96 (0.90-0.98)	0.97 (0.96-0.98)
LV mass, g	107	0.92 (0.88-0.94)	0.92 (0.88-0.94)
RVEF, %	107	0.73 (0.63-0.81)	0.74 (0.64-0.81)
RVEDV, ml	107	0.89 (0.72-0.94)	0.92 (0.88-0.94)
RVESV, ml	107	0.89 (0.75-0.94)	0.91 (0.88-0.94)
LGE, % of LV	51	0.94 (0.88-0.97)	0.94 (0.90-0.97)

2D = 2-dimensional; 3D = 3-dimensional; CI = confidence interval; ICC = intraclass correlation coefficient, LGE = late gadolinium enhancement; LV = left ventricle; LVEDV = left ventricular end-diastolic volume; LVEF = left ventricular ejection fraction; LVESV = left ventricular end-systolic volume; RVEDV = right ventricular end-diastolic volume; RVEF = right ventricular ejection fraction; RVESV = right ventricular end-systolic volume.

were manually traced to obtain right ventricular end-diastolic volume (RVEDV), right ventricular end-systolic volume (RVESV), and RVEF.

Scar extension was defined after manually tracing the endocardial and epicardial contours on LGE short-axis images. Abnormal areas were defined using the full width at half-maximum, with manual correction if needed. Any hypointense black areas within the necrotic zone, corresponding to MVO, were included within the necrotic area (8).

STATISTICAL METHODS. A detailed explanation of the statistical methods including sample-size calculation is described in the Supplemental Appendix. In brief, continuous variables are presented as mean ± SD or 95% confidence interval (CI). Agreement between 2D and 3D techniques was assessed with the intraclass correlation coefficient (ICC), Bland-Altman plots, Passing-Bablok regression analysis, and Lin's concordance correlation coefficients. Agreement was considered poor, moderate, good, or excellent for ICC <0.50, 0.50 to 0.75, 0.75 to 0.90, and >0.90, respectively. For Bland-Altman analysis, no significant systematic bias was assumed if 95% CI for the mean between-measurement difference contained the value 0. For Passing-Bablok regression analysis, no constant bias between measurements was assumed if 95% CI of the intercept included the value 0, whereas an absence of significant proportional bias was assumed if 95% CI of the intercept included the value 1. Lin's concordance correlation coefficients were computed to measure precision (Pearson's ρ) and accuracy (bias corrected factor). Because the interpretation is very similar, the same threshold values were used for Lin's concordance correlation coefficients as for ICC.

Intraobserver and interobserver agreement for 3D imaging were assessed using a similar strategy based on ICC and Bland-Altman analysis in separate random subsamples of 20 individuals from the total of valid 3D cine and LGE sequences. Statistical significance was set at $p < 0.05$. All statistical analyses were performed and graphs generated using STATA Version 15 (StataCorp, College Station, Texas).

RESULTS

PARTICIPANT FLOW DIAGRAM AND GENERAL CHARACTERISTICS. The study enrolled 121 participants (mean age 59.2 ± 10.9 years; 24% female). In total, 14 individuals were excluded, 6 for problems in 3D cine acquisition. Thus, 107 participants (mean age 58.3 ± 10.6 years; 24% female) were valid for cine analysis. Of this total, 51 patients (48%) showed some degree of myocardial contrast enhancement and were included in the LGE analysis (Figure 2).

In the group of patients undergoing 3D ultrafast protocol only, studies were properly acquired in all, with median (interquartile range) door-to-door time of 11 min 51 s (2 min 35 s). Cine 3D ESSOS sequence was repeated in 2 patients because the first scan obtained was of suboptimal image quality. Three-dimensional LGE sequence was repeated in 6 patients, mostly because the normal myocardium was not optimally nulled in the first scan. CMR studies of 2 participants undergoing 3D ultrafast protocol only are shown in Videos 2 and 3.

COMPARATIVE PERFORMANCE OF 3D ESSOS CINE AND 2D CINE. Mean acquisition time was 24 ± 1 s versus 280 ± 17 s for 3D and 2D cine imaging, respectively. Mean LVEF was 51 ± 12% by 3D cine and 52 ± 12% by 2D cine. ICC values for absolute-agreement and consistency-of-agreement between 3D ESSOS and 2D LVEF measures were both 0.96 (95% CI: 0.94 to 0.97) (Table 1). Mean bias between techniques for LVEF was −0.7% (95% CI: −1.4 to 0.0), with a lower limit of agreement of −7.4% (95% CI: −8.5 to −6.3) and an upper limit of agreement of 6.0% (95% CI: 4.9 to 7.1). Passing-Bablok regression analysis revealed no significant bias (Figure 3D). Detailed Bland-Altman and Passing-Bablok regression results from all 3D and 2D cine comparisons are given in Tables 2 and 3, and Supplemental Figure 5. Lin's concordance correlation coefficient between 3D ESSOS and 2D LVEF was 0.96 (95% CI: 0.94 to 0.97), showing excellent precision and accuracy (Table 4). Intraobserver variability for 3D cine quantifications was excellent, with mean differences (95% CI) of −0.7% (−1.5 to 0.1) for LVEF, 0.3 ml (−4.7 to 5.3) for

FIGURE 3 Comparisons Between 2D (Reference) and 3D CMR Measurements

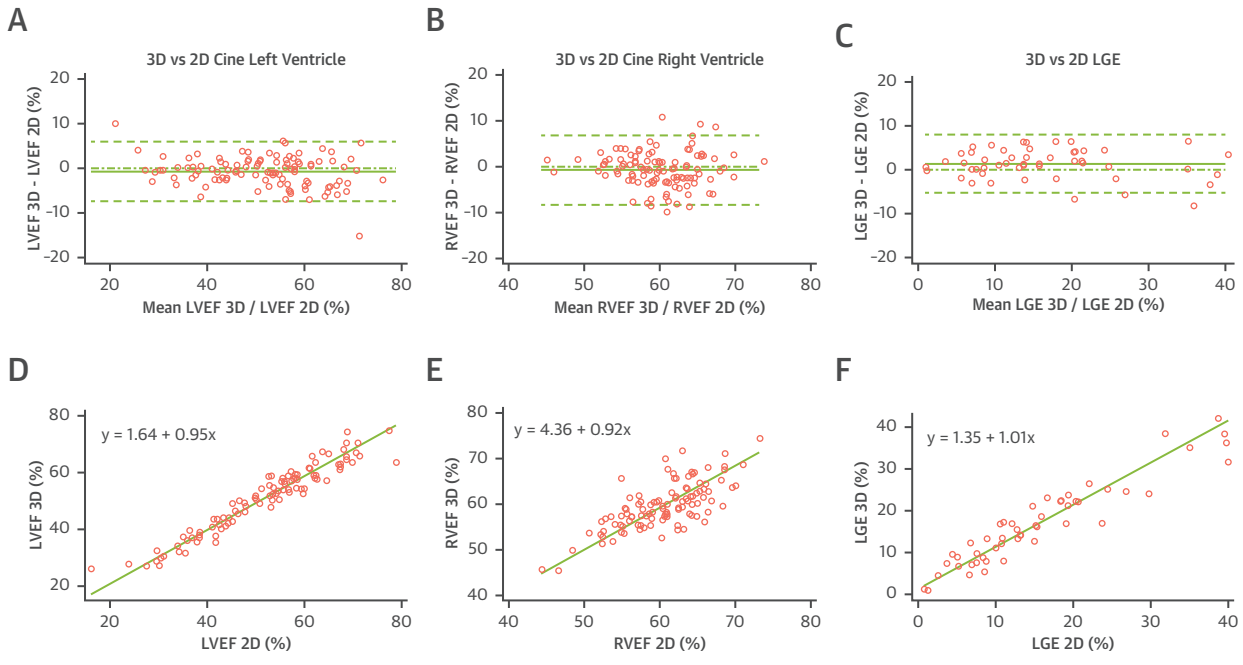

Bland-Altman plot **(A–C)** and Passing-Bablok regression **(D to F)** for comparisons between 2-dimensional (2D) and 3-dimensional (3D) cardiac magnetic resonance (CMR) measurements of left ventricular ejection fraction (LVEF) **(A, D)** and right ventricular ejection fraction (RVEF) **(B, E)** from cine and late gadolinium enhancement (LGE) **(C, F)**.

LVEDV, and 1.6 ml (−1.5 to 4.6) for LVESV. Interobserver variability for 3D ESSOS cine quantifications was equally good, with mean differences (95% CI) of −0.2% (−1.4 to 1.1) for LVEF, 0.3 ml (−5.4 to 6.0) for LVEDV, and 0.3 ml (-3.3 to 3.9) for LVESV.

Wall thickening analysis was performed in 51 patients who showed enhanced regions on LGE. A total of 816 LV segments was evaluated in the 3D and 2D cine images. Mean LV wall thickening was 2.2 ± 2.2 by 3D and 2D, respectively. Mean bias (95% CI) was 0.2 (0.0 to 0.3). Supplemental Figure 5 shows Bland-Altman plots and Passing-Bablok regression for regional contractility analyses in 3D versus 2D.

Mean RVEF was 59.7 ± 5.2% by 3D and 60.4 ± 5.4% by 2D cine. ICC values for absolute-agreement and consistency-of-agreement between 3D and 2D RVEF measures were 0.73 (95% CI: 0.63 to 0.81) and 0.74 (95% CI: 0.64 to 0.81), respectively (**Table 1**). Mean bias between techniques for RVEF was −0.7% (95% CI: −1.4 to 0.0), with a lower limit of agreement of −8.2% (95% CI: −9.5 to −6.9) and an upper limit of agreement of 6.8% (95% CI: 5.5 to 8.1). Passing-Bablok regression analysis revealed no significant bias (**Figure 3E**). Detailed Bland-Altman and Passing-Bablok regression results from all 3D and 2D cine comparisons are given in **Tables 2 and 3 and** Supplemental Figure 1. Lin's concordance correlation coefficient between 3D and 2D RVEF was 0.73 (95% CI: 0.64 to 0.87), showing good precision and excellent accuracy (**Table 4**). Intraobserver variability for 3D cine quantifications also was excellent for RV, with mean differences (95% CI) of 0.3% (−0.5 to 1.1) for RVEF, −5.0 ml (−10.3 to 0.2) for RVEDV, and −2.5 ml (−5.0 to 0.0) for RVESV. Interobserver variability for 3D cine quantifications was equally good, with mean differences (95% CI) of -2.1% (−4.1 to −0.1) for RVEF, −5.6 ml (−12.5 to 1.4) for RVEDV, and 1.0 ml (−2.8 to 4.8) for RVESV.

All observer variabilities and agreements for 3D cine imaging analyses for LV and RV are listed in Supplemental Tables 1 to 4.

All conventional 2D cine studies received an image quality score of 4 (very good image quality). Of the 3D images, 91% (97 of 107) were scored as 3 (good image quality) due to slightly less image resolution of the 3D MPR images. In 9% (10 of 107) of the 3D cine images, image quality was scored as 2 (regular) due to minor remaining residual artifacts after static subtraction. Of the 3D LGE images, 65% (33 of 51) were scored as 4 (very good image quality); 25% (13 of 51) were scored

FIGURE 4 3D and 2D Cine and LGE Acquisition in the Same Patient

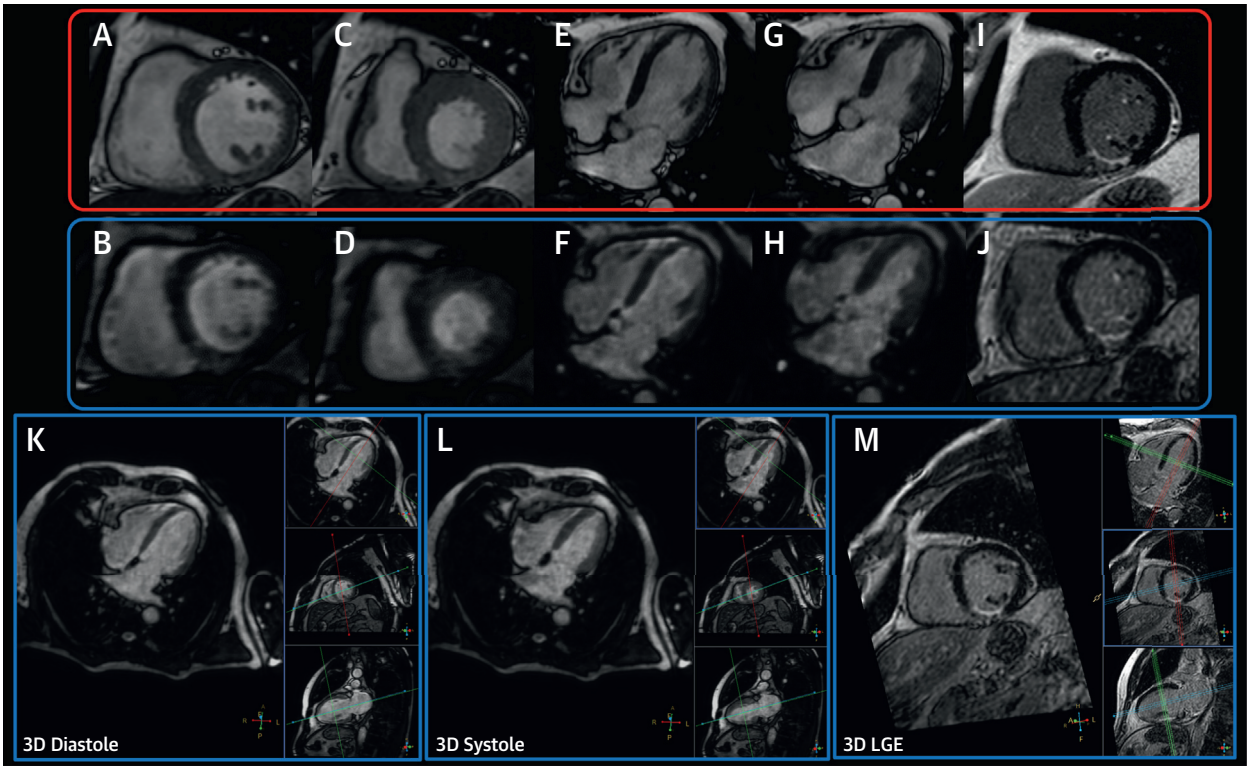

(A, B) Two-dimensional (2D) and 3-dimensional (3D) end-diastolic short-axis cine views. **(C, D)** Two-dimensional and 3D end-systolic short-axis cine views. **(E, F)** Two-dimensional and 3D end-diastolic 4-chamber long-axis cine views. **(G, H)** End-systolic 4-chamber long-axis cine views. **(I, J)** 2D and 3D late gadolinium enhancement (LGE) end-diastolic short-axis views. **(K to M)** Three-dimensional and 3D LGE cine workflow used to obtain images in short-axis, 4-chamber long axis, and 2-chamber long-axis views.

as 3 (good image quality) due to slightly noise amplification in the short axis MPR images; and 10% (5 of 51) were scored as 2 due to movement artifact in the heart region caused be cardiac frequency changes during 3D acquisition. A complete example case can be seen in **Figure 4** and an example of IQ level for cine and LGE images is shown in Supplemental Figure 6.

COMPARATIVE PERFORMANCE OF 3D LGE AND 2D LGE. Mean acquisition time for single breath-hold 3D LGE scans and multislice 2D LGE scans were 22 ± 1 s and 280 ± 17 s, respectively. Mean LGE (% LV) as assessed by 3D and 2D imaging was 17.0 ± 9.9% and 15.7 ± 10.4%, respectively. ICC values for absolute-agreement and consistency-of-agreement between 3D and 2D LGE measurements were 0.94 (95% CI: 0.88 to 0.97) and 0.94 (95% CI: 0.90 to 0.97), respectively (**Table 1**). Mean between-technique bias for LGE was 1.3% (95% CI: 0.3 to 2.2), with a lower limit of agreement of -5.3% (95% CI: −7.0 to −3.7) and an upper limit of agreement of 7.9% (95% CI: 6.3 to 9.6) (**Table 2**). Passing-Bablok regression analysis revealed no significant bias (**Table 3, Figure 3B**). Lin's concordance correlation coefficient between 3D and 2D LGE was 0.94 (95% CI: 0.90 to 0.97), showing excellent precision and accuracy (**Table 4**). Intraobserver agreement for 3D LGE quantification was very good, with a mean difference (95% CI) of 0.8% LV (−0.3 to 2.0). Interobserver variability for 3D LGE quantifications was equally good, with a mean difference (95% CI) of −0.9% LV (−2.9 to 1.2). All 3D LGE observer variables are listed in Supplemental Tables 5 and 6. In addition, it was confirmed that the spatial LGE distribution of 2D and 3D techniques matched in all cases.

DISCUSSION

The long duration (≥30 min) of standard clinical CMR protocols (cine+LGE) (9) imposes time constraints, presents a cost barrier, and causes patient discomfort,

CENTRAL ILLUSTRATION 3-Dimensional Ultrafast Cardiac Magnetic Resonance Protocol

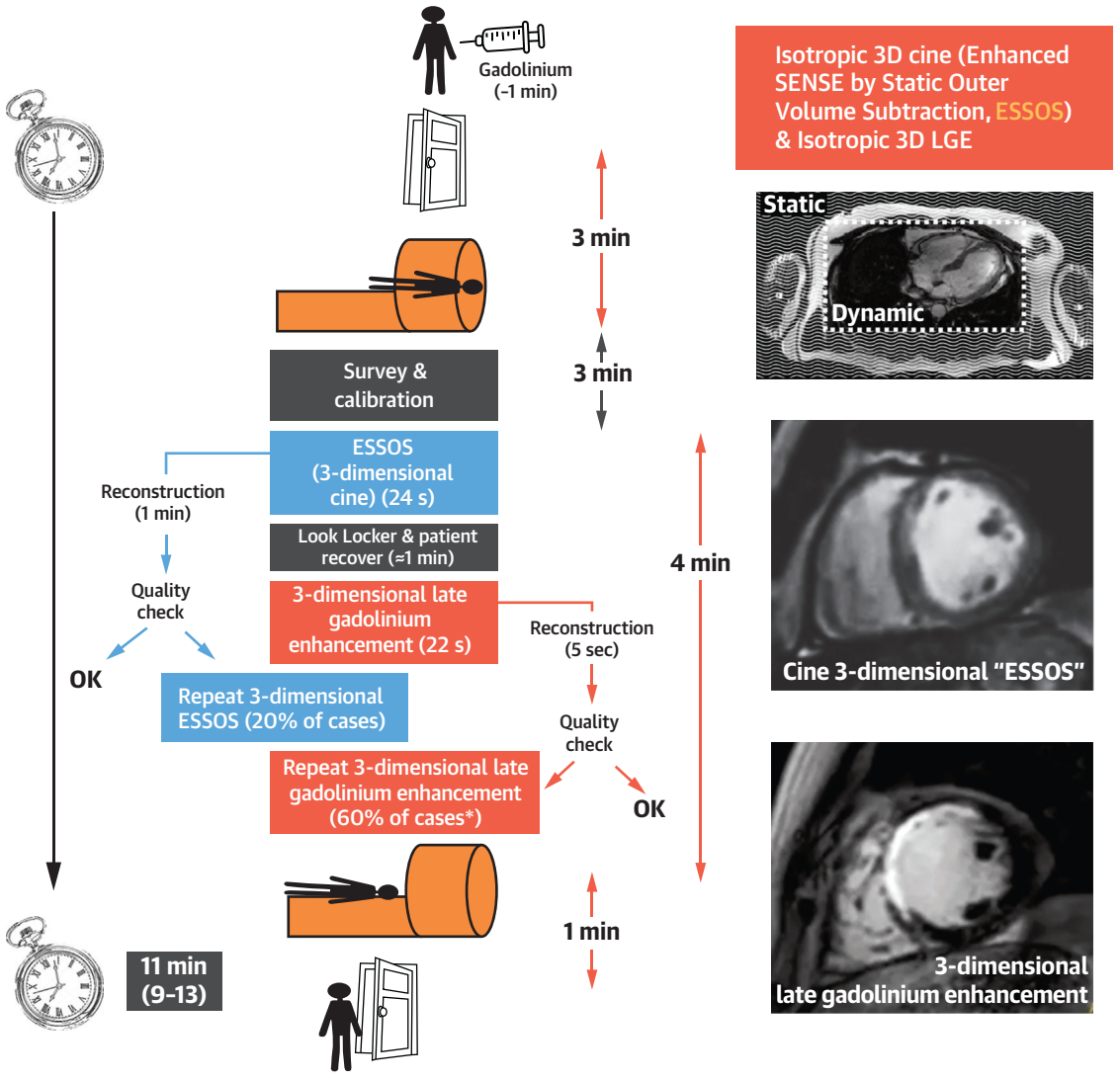

Gómez-Talavera, S. et al. J Am Coll Cardiol Img. 2021;14(9):1742–1754.

The ultrafast protocol is based on the newly developed cine 3-dimensional (3D) ESSOS sequence (whole-heart volume acquired in 1 breath-hold) plus 3D late gadolinium enhancement (LGE) (whole-heart volume acquired in 1 breath-hold). Contrast agent is injected outside the magnet. Door to door includes the time for patient positioning, calibrations, ultrafast sequences, and patient extraction. Because reconstruction is done in the cardiac magnetic resonance workstation, ultrafast sequences can be repeated if the quality is suboptimal. *Most frequent cause for repeating 3D LGE was suboptimal normal myocardium nulling in the first scan.

all of which act as brakes on a more generalized uptake of CMR imaging. The present study provides clinical validation of a 3D ultrafast CMR protocol with an acquisition period of <1 min. The new CMR protocol assesses the clinically most relevant cardiac parameters, including anatomy (LV and RV volumes and LV mass), function (LVEF and RVEF), and presence and extent of LGE (**Central Illustration**). The protocol consists of two 3D sequences, each capable of acquiring the whole heart with isotropic resolution in just 1 breath-hold. The single breath-hold 3D ESSOS cine sequence is tested here for the first time (for extended technical information, see the Supplemental Appendix). The single breath-hold 3D LGE sequence has been used by other investigators (10); however, this study provides the first validation of a 3D LGE

TABLE 2 Bias and Lower and Upper Limits of Agreement From Bland-Altman Plots and 95% CI for Comparisons Between 2D (Reference) and 3D Cine and LGE Measurements

				Bland-Altman Plot		
Measured Variable	n	2D CMR	3D CMR	Bias (95% CI)	Lower Limit of Agreement (95% CI)	Upper Limit of Agreement (95% CI)
LVEF, %	107	51.7 ± 12.4	51.0 ± 11.6	−0.7 (−1.4 to 0.0)	−7.4 (−8.5 to −6.3)	6.0 (4.9 to 7.1)
LVEDV, ml	107	191.9 ± 56.4	202.7 ± 59.1	10.8 (7.3 to 14.3)	−25.0 (−31.0 to −18.9)	46.5 (40.5 to 52.6)
LVESV, ml	107	96.1 ± 48.1	103.3 ± 50.6	7.2 (5.1 to 9.3)	−14.7 (−18.4 to −11.0)	29.1 (25.4 to 32.8)
LV mass, g	107	99.9 ± 37.8	99.5 ± 39.0	−0.5 (−3.4 to 2.5)	−30.9 (−36.1 to −25.8)	30.0 (24.8 to 35.1)
RVEF, %	107	60.4 ± 5.4	59.7 ± 5.2	−0.7 (−1.4 to 0.0)	−8.2 (−9.5 to −6.9)	6.8 (5.5 to 8.1)
RVEDV, ml	107	143.6 ± 40.5	154.8 ± 45.4	11.2 (7.8 to 14.6)	−23.3 (−29.1 to −17.4)	45.7 (39.8 to 51.5)
RVESV, ml	107	57.9 ± 21.5	63.3 ± 22.7	5.5 (3.7 to 7.2)	−12.5 (−15.5 to −9.4)	23.4 (20.3 to 26.4)
LGE, % of LV	51	15.7 ± 10.4	17.0 ± 9.9	1.3 (0.3 to 2.2)	−5.3 (−7.0 to −3.7)	7.9 (6.3 to 9.6)

Values are mean ± SD, unless otherwise indicated.
CMR = cardiac magnetic resonance; other abbreviations as in Table 1.

sequence with isotropic resolution. The validated CMR protocol shows overall very good reliability and agreement with the standard methodology, as well as excellent intraobserver and interobserver agreements. Moreover, image reconstruction is performed in close to real time, facilitating implementation in daily practice. Although the proposed protocol includes new technical developments for 3D cine acquisition, it does not require any specific hardware upgrade, and it has demonstrate its utility with very standard 16-channel phased-array coil. Measuring cardiac anatomy, function, and LGE has significant benefits for prognosis and patient management (1,11). Therefore, by largely expanding the indication of CMR, this 3D ultrafast protocol has enormous potential to benefit patients while increasing their comfort and reducing associated costs. The proposed ultrafast protocol can be applied to patients with heart diseases for which other rapid protocols, including more conventional techniques, have demonstrated clinical benefit (cardiomyopathy, chronic ischemic heart disease, and hypertensive heart disease [4]). As an improvement to this rapid protocol, the proposed protocol will simplify the overall examination workflow, potentially reducing the scan time to 3 breath-holds, including look-locker scan (12). In addition, the proposed 3D technique has been validated to assess RV anatomy and function, thus extending its application to other pathologies such as pulmonary hypertension, with similar reproducibility reported in previous works (22). Although this concept has not yet been demonstrated, the proposed 3D approach could improve overall clinical performance for complex anatomies, such as congenital heart diseases, or include the evaluation of big vessel anatomies, such as the aorta or pulmonary artery, in the imaging report.

TABLE 3 Intercept, Slope, and Residual SD of Passing-Bablok Regression for Comparisons Between 2D (Reference) and 3D Cine and LGE Measurements

		Passing-Bablok Regression		
Measured Variable	n	Intercept (95% CI)	Slope (95% CI)	Residual SD (95% CI)
LVEF, %	107	1.64 (−0.91 to 4.03)	0.95 (0.90-1.01)	3.42 (−6.70 to 6.70)
LVEDV, ml	107	2.07 (−10.03 to 14.81)	1.04 (0.97-1.11)	18.24 (−35.75 to 35.75)
LVESV, ml	107	2.00 (−2.33 to 6.61)	1.05 (1.00-1.11)	11.18 (−21.91 to 21.91)
LV mass, g	107	−2.25 (−10.70 to 5.97)	1.03 (0.93-1.12)	15.54 (−30.46 to 30.46)
RVEF, %	107	4.36 (−4.15 to 11.96)	0.92 (0.78-1.06)	3.84 (−7.52 to 7.52)
RVEDV, ml	107	−1.15 (−14.14 to 13.26)	1.09 (0.99-1.19)	17.59 (−34.47 to 34.47)
RVESV, ml	107	1.45 (−4.41 to 5.82)	1.06 (0.98-1.16)	9.14 (−17.91 to 17.91)
LGE, % of LV	51	1.35 (−0.43 to 2.97)	1.01 (0.90-1.12)	3.38 (−6.63 to 6.63)

Abbreviations as in Table 1.

RECENT TECHNICAL ADVANCES IN ACCELERATED CMR PROTOCOLS. Standard clinical measurement of LV and RV anatomy and function by CMR involves the time-consuming acquisition of a stack of slices in double-oblique short-axis and long-axis orientations. The 2D slices are acquired sequentially, with typically only 1 or 2 slices per breath-hold. Additional time is required for planning the double-oblique slices as well as patient recovery between breath-holds. For these reasons, there is a great interest in developing a highly accelerated cardiac cine acquisition method that allows nonangulated 3D acquisition of the entire heart in a single breath-hold, with sufficient isotropic spatial resolution to allow subsequent reformatting in any desired oblique orientation.

Latest generation of acceleration techniques, based on compressed sensing theory, can achieve even higher acceleration factors, allowing acquisition of 3D short-axis cine volumes in a single breath-hold with isotropic resolution (6,13–15). Unfortunately, compressed sensing techniques require very long

reconstruction times (>10 min), which impede their implementation in routine clinical practice.

Single breath-hold acquisitions have also been proposed for 3D LGE, as methods developed to date have not allowed isotropic resolution, even with very long breath-holds (16). Proposed improvements to LGE sequences have focused on accelerating high-resolution navigator triggered acquisitions, with a maximum acceleration factor of 4 (17).

ADVANTAGES OF THE NEW ACCELERATED CMR PROTOCOL. This study proposes the newly developed 3D ESSOS cine sequence as an efficient technique that combines SENSE with static outer volume suppression. ESSOS enables acquisition of a whole-chest 3D coronal volume with 2.6-mm isotropic resolution and 16 cardiac phases in a single breath-hold (net acceleration factor of 34) (Videos 4, 5, 6, and 7). Whole-chest acquisitions with isotropic resolution allow assessment of cardiac function as well as of the anatomy of the large vessels (aorta and pulmonary veins). In addition, nonangulated whole-chest isotropic 3D coronal acquisitions remove the need for prospective planning of the desired cardiac orientations (e.g., short axis) based on pre-scan scout images, as required in conventional 2D double-oblique imaging. This simplifies and improves the overall cardiac CMR acquisition workflow. Finally, the use of nonselected pulses in ESSOS reduces the sequence TR, which not only shortens the total acquisition but also the sensitivity of the SSFP sequence to off-resonance effects, which is particularly challenging at 3.0-T (18).

Three-dimensional short-axis volumes of the whole heart can also be acquired in a single breath-hold given recent advances in compressed sensing techniques. This approach yields a volume thickness of 15 cm and gives good spatial and temporal resolution ($1.6 \times 1.9 \times 2.3$ mm^3 and 48 ms, respectively) (15). However, the breath-hold is very long (32 ± 7 s), and the reported reconstruction time is approximately 10 min, whereas ESSOS reconstruction time for a full 3D cine dataset at the scanner is approximately 1 min. This fast reconstruction is possible because ESSOS uses conventional (noniterative) SENSE reconstruction combined with computationally simple operations such as multiplication and subtraction.

ESSOS also works for acquisition without contrast administration (Supplemental Figure 7), but the blood signal saturation due to 3D excitation pulses produces suboptimal delineation of endocardial borders. Although this problem is shared by all 3D cine techniques, for ESSOS it is even more severe because it used nonselected pulses. In addition, in the present work only 3-T acquisitions have been shown, for which this blood signal saturation effect is even stronger.

TABLE 4 Concordance Correlation Analysis Between 2D and 3D Cine and LGE Measurements

Measured Variable	n	Concordance Correlation Analysis		
		Lin's r_{ccc} (95% CI)	Precision ρ	Accuracy C_b
LVEF, %	107	0.96 (0.94–0.97)	0.96	>0.99
LVEDV, ml	107	0.93 (0.91–0.96)	0.95	0.98
LVESV, ml	107	0.96 (0.95–0.98)	0.98	0.99
LV mass, g	107	0.92 (0.89–0.95)	0.92	>0.99
RVEF, %	107	0.73 (0.64–0.82)	0.74	0.99
RVEDV, ml	107	0.89 (0.85–0.92)	0.92	0.96
RVESV, ml	107	0.89 (0.85–0.93)	0.92	0.97
LGE, % of LV	51	0.94 (0.90–0.97)	0.95	0.99

Accuracy C_b values ≥0.995 are indicated as >0.99, not rounded to 1.00.
Abbreviations as in Table 1.

For LGE imaging, sagittal orientation of the 3D volume allows an acceleration factor of 4, which is comparable to those already reported in the published data. This 3D acquisition allows evaluation of enhanced regions from any orientation without further acquisition. Another advantage of this 3D approach is the elimination of the partial volume effects of 2D acquisitions. In addition, data acquisition without the need for orientation simplified the training of the scanner operators. One potential limitation could be the difficulty in implementing this sequence in a single breath-hold with state-of-the-art phase sensitive inversion recovery techniques (19). This could be minimized by selecting the correct inversion time using a look-locker sequence before the 3D protocol, extending the protocol to an additional breath-hold.

RELIABILITY AND AGREEMENT OF THE VALIDATED METHODOLOGY. The image quality obtained with the ESSOS technique translated into very good agreement between 3D and 2D cine measurements. The documented observer variability was comparable to the reproducibility obtained with the standard (2D) technique (20–22) and other validation studies using accelerated approaches (6,23), with most of the observer variability in ESSOS resulting from discrepancies in the definition of the basal-most

short-axis slices (24). Despite the overall good agreement and reliability between 3D and 2D LGE measures, 3D LGE imaging tended to slightly overestimate the LGE area. This can be explained, at least in part, by the relatively lower in-plane resolution of 3D LGE imaging. Because 2D LGE was acquired at the end of the imaging protocol, another possible factor is delayed washout in the diseased myocardium. Nevertheless, the variability observed in LGE imaging is similar to that previously reported in recent studies validating other 3D LGE single breath-hold methods (25).

STUDY LIMITATIONS. A potential limitation of 3D ESSOS cine is the contrast-based nature of the sequence. Although ESSOS also works for acquisition without contrast administration (Supplemental Figure 6), the blood signal saturation due to 3D excitation pulses produces suboptimal delineation of endocardial borders. This problem is shared by all 3D cine techniques but for ESSOS is even more severe because the entire signal from the chest is saturated due to use of nonselected pulses. However, given that most patients undergoing CMR undergo LGE evaluation, this limitation should be restricted to patients with a formal contraindication to gadolinium administration (e.g., severe renal insufficiency).

The proposed protocol has been tested at 3.0-T field strength, and further validation will be required for more stablished 1.5-T systems with lower signal to noise. To compensate for this loss in signal, higher flip angles can be used for ESSOS, as lower energy deposition of the excitation pulses at this magnetic field strength does not increase sequence TR. As an additional impact, higher flip angles could benefit the contrast between the blood pool and heart muscle in cases in which contrast media cannot be administered. In the case of 3D LGE, this signal loss can be compensated using SSFP readout techniques, which is more suitable for lower magnetic fields and provides significantly higher signal compared with spoiled TFE technique.

Three-dimensional ESSOS cine acquisition requires a breath-hold of approximately 24 s. Although most individuals can tolerate this, such long breath-holds may not be achievable for some patients. In recent implementations of the sequence, the research team managed to reduce breath-hold to <15 s with no significant loss of resolution; however, this shorter protocol was not attempted in the cohort reported here. This protocol does not include CMR mapping techniques able to track the dynamics of complex pathophysiological processes occurring after myocardial infarction and other pathophysiological processes (26–29). Nevertheless, mapping sequences could be implemented before contrast administration at the cost of increasing total protocol time. For validation purposes, we performed contrast administration after the acquisition of 2D cine imaging. However, for clinical practice implementation of the present protocol, contrast could be administered with the patient positioned on the bed or even outside the magnet, dramatically shortening patient time inside the scanner. It should be highlighted that when parametric acquisitions (e.g., native T1, T2, or T2* mapping) are planned, they should be performed before injection of the contrast agent. This will significantly extend the study, not just by the time of mapping acquisition but also the 10-min lag between contrast injection and 3D ESSOS and 3D LGE acquisition (30,31).

CONCLUSIONS

This study provides clinical validation of a 3D ultrafast CMR protocol to evaluate the most important cardiac anatomy and function parameters with isotropic resolution. The present study validates both protocol components: the new single breath-hold 3D ESSOS cine sequence and the single breath-hold 3D LGE sequence improved with isotropic resolution. The protocol combines total acquisition time to <1 min with reconstruction almost in real time, thus facilitating implementation in daily practice. The protocol can be implemented in any commercially available clinical magnetic resonance equipment. Incorporation of this ultrafast protocol could hugely expand the indication for CMR, providing benefits to patients while increasing their comfort and reducing associated costs.

ACKNOWLEDGMENTS The authors would like to thank Noemi Escalera for coordinating the study, and CNIC imaging technologists Angel Macías and Marta Gavilán for their support with image acquisition. Simon Bartlett provided English editing.

FUNDING SUPPORT AND AUTHOR DISCLOSURES

Funding included Instituto de Salud Carlos III (ISCIII) and the European Regional Development Fund (ERDF) Grants DTS17/00136 to Dr. Ibáñez and PI19/01704 to Dr. Fernandez-Jimenez; Spanish Society of Cardiology Translational Research Grant 2016 to Dr. Ibáñez; European Research Council ERC-CoG 819775-MATRIX to Dr. Ibáñez; Comunidad de Madrid S2017/BMD-3867-RENIM-CM to Drs. Desco and Ibáñez; and Ministerio de Ciencia e Innovación (MICINN) RETOS2019-107332RB-I00 to Dr. Ibáñez. Dr. Fernandez-Jimenez

received funding from the European Union Horizon 2020 research and innovation programme under Marie Skłodowska-Curie Hrant Agreement No. 707642. The CNIC is supported by the ISCIII, the MICINN, and the Pro CNIC Foundation. Drs. Fernandez-Jimenez, Nothnagel, Fuster, Ibáñez, and Javier Sánchez-González are inventors of a joint patent (Philips/CNIC) for the new cine imaging method here described and validated/protected under the IP #2014P00960EP. Drs. Nothnagel, Kouwenhoven, Clemence, and Javier Sánchez-González are Philips employees. All other authors have reported that they have no relationships relevant to the contents of this paper to disclose.

ADDRESS FOR CORRESPONDENCE: Dr. Javier Sánchez-González, Philips Healthcare Iberia, María Portugal, 1, 29050 Madrid, Spain. E-mail: Javier.Sanchez.Gonzalez@philips.com. OR Dr. Borja Ibanez, Centro Nacional de Investigaciones Cardiovasculares Carlos III (CNIC), Melchor Fernandez Almagro, 3, 28029 Madrid, Spain. E-mail: bibanez@cnic.es.

PERSPECTIVES

COMPETENCY IN MEDICAL KNOWLEDGE: CMR is the reference tool for assessing cardiac anatomy and function; however, its use is limited due to time and cost constraints. We clinically validated a 3D ultrafast CMR isotropic protocol comprising a new single breath-hold 3D cine sequence (ESSOS) and an updated single breath-hold 3D LGE sequence. The new protocol acquires the major cardiac parameters, including ejection fraction and extent of injured myocardium, in <1 min with near–real-time image reconstruction.

TRANSLATIONAL OUTLOOK: Implementation of this ultrafast protocol could hugely expand the indication for CMR, providing benefits to patients while increasing their comfort and reducing associated costs.

REFERENCES

1. Ibanez B, Aletras AH, Arai AE, et al. Cardiac MRI endpoints in myocardial infarction experimental and clinical trials: JACC scientific expert panel. *J Am Coll Cardiol*. 2019;74:238–256.

2. El Aidi H, Adams A, Moons KG, et al. Cardiac magnetic resonance imaging findings and the risk of cardiovascular events in patients with recent myocardial infarction or suspected or known coronary artery disease: a systematic review of prognostic studies. *J Am Coll Cardiol*. 2014;63:1031–1045.

3. Puntmann VO, Valbuena S, Hinojar R, et al. Society for Cardiovascular Magnetic Resonance (SCMR) expert consensus for CMR imaging endpoints in clinical research: part I—analytical validation and clinical qualification. *J Cardiovasc Magn Reson*. 2018;20:67.

4. Kramer CM, Barkhausen J, Bucciarelli-Ducci C, Flamm SD, Kim RJ, Nagel E. Standardized cardiovascular magnetic resonance imaging (CMR) protocols: 2020 update. *J Cardiovasc Magn Reson*. 2020;22:17.

5. Goetti R, Kozerke S, Donati OF, et al. Acute, subacute, and chronic myocardial infarction: quantitative comparison of 2D and 3D late gadolinium enhancement MR imaging. *Radiology*. 2011;259:704–711.

6. Vincenti G, Monney P, Chaptinel J, et al. Compressed sensing single-breath-hold CMR for fast quantification of LV function, volumes, and mass. *J Am Coll Cardiol Img*. 2014;7:882–892.

7. Cerqueira MD, Weissman NJ, Dilsizian V, et al. Standardized myocardial segmentation and nomenclature for tomographic imaging of the heart. A statement for healthcare professionals from the Cardiac Imaging Committee of the Council on Clinical Cardiology of the American Heart Association. *Circulation*. 2002;105:539–542.

8. Fernandez-Jimenez R, Barreiro-Perez M, Martin-Garcia A, et al. Dynamic edematous response of the human heart to myocardial infarction: implications for assessing myocardial area at risk and salvage. *Circulation*. 2017;136:1288–1300.

9. Demirkiran A, Everaars H, Amier RP, et al. Cardiovascular magnetic resonance techniques for tissue characterization after acute myocardial injury. *Eur Heart J Cardiovasc Imaging*. 2019;20:723–734.

10. Viallon M, Jacquier A, Rotaru C, et al. Head-to-head comparison of eight late gadolinium-enhanced cardiac MR (LGE CMR) sequences at 1.5 tesla: from bench to bedside. *J Magn Reson Imaging*. 2011;34:1374–1387.

11. Bruder O, Wagner A, Lombardi M, et al. European Cardiovascular Magnetic Resonance (EuroCMR) registry—multi national results from 57 centers in 15 countries. *J Cardiovasc Magn Reson*. 2013;15:9.

12. Menacho K, Ramirez S, Segura P, et al. INCA (Peru) study: impact of non-invasive cardiac magnetic resonance assessment in the developing world. *J Am Heart Assoc*. 2018;7:e008981.

13. Jung H, Sung K, Nayak KS, Kim EY, Ye JC. k-t FOCUSS: a general compressed sensing framework for high resolution dynamic MRI. *Magn Reson Med*. 2009;61:103–116.

14. Wech T, Pickl W, Tran-Gia J, et al. Whole-heart cine MRI in a single breath-hold—a compressed sensing accelerated 3D acquisition technique for assessment of cardiac function. *Rofo*. 2014;186:37–41.

15. Wetzl J, Schmidt M, Pontana F, et al. Single-breath-hold 3-D CINE imaging of the left ventricle using Cartesian sampling. *MAGMA*. 2018;31:19–31.

16. Roujol S, Basha TA, Akcakaya M, et al. 3D late gadolinium enhancement in a single prolonged breath-hold using supplemental oxygenation and hyperventilation. *Magn Reson Med*. 2014;72:850–857.

17. Basha TA, Akcakaya M, Liew C, et al. Clinical performance of high-resolution late gadolinium enhancement imaging with compressed sensing. *J Magn Reson Imaging*. 2017;46:1829–1838.

18. Schar M, Kozerke S, Fischer SE, Boesiger P. Cardiac SSFP imaging at 3 Tesla. *Magn Reson Med*. 2004;51:799–806.

19. Kellman P, Arai AE, McVeigh ER, Aletras AH. Phase-sensitive inversion recovery for detecting myocardial infarction using gadolinium-delayed hyperenhancement. *Magn Reson Med*. 2002;47:372–383.

20. Danilouchkine MG, Westenberg JJ, de Roos A, Reiber JH, Lelieveldt BP. Operator induced variability in cardiovascular MR: left ventricular measurements and their reproducibility. *J Cardiovasc Magn Reson*. 2005;7:447–457.

21. Grothues F, Smith GC, Moon JC, et al. Comparison of interstudy reproducibility of cardiovascular magnetic resonance with two-dimensional echocardiography in normal subjects and in patients with heart failure or left ventricular hypertrophy. *Am J Cardiol*. 2002;90:29–34.

22. Mooij CF, de Wit CJ, Graham DA, Powell AJ, Geva T. Reproducibility of MRI measurements of right ventricular size and function in patients with normal and dilated ventricles. *J Magn Reson Imaging*. 2008;28:67–73.

23. Jeong D, Schiebler ML, Lai P, Wang K, Vigen KK, Francois CJ. Single breath hold 3D cardiac cine MRI using kat-ARC: preliminary results at 1.5T. *Int J Cardiovasc Imaging*. 2015;31:851–857.

24. Simprini LA, Goyal P, Codella N, et al. Geometry-independent inclusion of basal myocardium yields improved cardiac magnetic resonance agreement with echocardiography and necropsy quantified left-ventricular mass. *J Hypertens*. 2013;31:2069–2076.

25. Foley JRJ, Fent GJ, Garg P, et al. Feasibility study of a single breath-hold, 3D mDIXON pulse

sequence for late gadolinium enhancement imaging of ischemic scar. *J Magn Reson Imaging*. 2019;49:1437–1445.

26. Galan-Arriola C, Lobo M, Vilchez-Tschischke JP, et al. Serial magnetic resonance imaging to identify early stages of anthracycline-induced cardiotoxicity. *J Am Coll Cardiol*. 2019;73:779–791.

27. Fernandez-Jimenez R, Galan-Arriola C, Sanchez-Gonzalez J, et al. Effect of ischemia duration and protective interventions on the temporal dynamics of tissue composition after myocardial infarction. *Circ Res*. 2017;121:439–450.

28. Fernandez-Jimenez R, Sanchez-Gonzalez J, Aguero J, et al. Myocardial edema after ischemia/reperfusion is not stable and follows a bimodal pattern: imaging and histological tissue characterization. *J Am Coll Cardiol*. 2015;65:315–323.

29. Fernandez-Jimenez R, Garcia-Prieto J, Sanchez-Gonzalez J, et al. Pathophysiology underlying the bimodal edema phenomenon after myocardial ischemia/reperfusion. *J Am Coll Cardiol*. 2015;66:816–828.

30. Fernandez-Jimenez R, Sanchez-Gonzalez J, Aguero J, et al. Fast T2 gradient-spin-echo (T2-GraSE) mapping for myocardial edema quantification: first in vivo validation in a porcine model of ischemia/reperfusion. *J Cardiovasc Magn Reson*. 2015;17:92.

31. Messroghli DR, Moon JC, Ferreira VM, et al. Clinical recommendations for cardiovascular magnetic resonance mapping of T1, T2, T2* and extracellular volume: a consensus statement by the Society for Cardiovascular Magnetic Resonance (SCMR) endorsed by the European Association for Cardiovascular Imaging (EACVI). *J Cardiovasc Magn Reson*. 2017;19:75.

KEY WORDS accelerated protocol, contrast media, gadolinium, heart, magnetic resonance, myocardium

APPENDIX For an expanded Methods section and supplemental figures, tables, and videos, please see the online version of this paper.